Research Article

Open Access

Gemma Rius*, Francesc Perez-Murano, Masamichi Yoshimura

Graphene crystal growth by thermal precipitation of focused ion beam induced deposition of carbon precursor via patterned-iron thin layers

Abstract: Recently, relevant advances on graphene as a building block of integrated circuits (ICs) have been demonstrated. Graphene growth and device fabrication related processing has been steadily and intensively powered due to commercial interest; however, there are many challenges associated with the incorporation of graphene into commercial applications which includes challenges associated with the synthesis of this material. Specifically, the controlled deposition of single layer large single crystal graphene on arbitrary supports, is particularly challenging. Previously, we have reported the first demonstration of the transformation of focused ion beam induced deposition of carbon (FIBID-C) into patterned graphitic layers by metal-assisted thermal treatment (Ni foils). In this present work, we continue exploiting the FIBID-C approach as a route for graphene deposition. Here, thin patterned Fe layers are used for the catalysis of graphenization and graphitization. We demonstrate the formation of high quality single and few layer graphene, which evidences, the possibility of using Fe as a catalyst for graphene deposition. The mechanism is understood as the minute precipitation of atomic carbon after supersaturation of some iron carbides formed under a high temperature treatment. As a consequence of the complete wetting of FIBID-C and patterned Fe layers, which enable graphene growth, the as-deposited patterns do not preserve their original shape after the thermal treatment.

Keywords: graphene, FIBID, iron catalyst, thermal treatment, crystallization

1 Introduction

Recently, relevant advances of graphene as a building block of integrated circuits (ICs) have been demonstrated [1]. Specifically, graphene has been employed as both an active and passive element of various device components. In particular, graphene-based transistors showed more than a 50% increase in efficiency relative to conventional transistors, while being smaller. Nevertheless, the interest in graphene relies on its versatility for a diverse range of potential applications that would benefit from graphenes' intrinsic characteristics [2]. Fundamental research of graphene has had important spin-offs in graphene related applications. Superior as well as especial in terms of (opto) electronic, mechanical and thermal properties, being graphene an all surface atoms material environment, e.g. substrate, does strongly influence its actual functional / practical characteristics [3].

Broadly speaking, the bottleneck in graphene arises from challenges associated with the synthesis; particularly, when well-determined material is required, for example, single layer large single crystal graphene [4]. Although graphitic carbon is the more stable form of carbon, in typical processing conditions, strict control of the deposition encounters many difficulties. In terms of its crystal growth, it is not only important to be able to generate large in-plane perfect crystals, but to prevent/ determine its out-of-plane growth (*i.e.* increase or selection of the number layers). As a result, a variety of synthesis approaches are being tested and developed beyond the original strategy to isolate graphene, namely the impractical mechanical exfoliation technique [5,6]. Techniques for obtaining graphene include: chemical vapor deposition (CVD), epitaxial graphene growth on SiC, or reduction of graphene oxide; each of these techniques

*Corresponding author: Gemma Rius: Nagoya Institute of Technology, NITech, Gokiso, Showa, 466-8555 Nagoya, Japan, E-mail: rius.gemma@nitech.ac.jp
Francesc Perez-Murano: Institut de Microelectronica de Barcelona, IMB-CNM-CSIC, Campus UAB, 08193, Bellaterra, Spain
Masamichi Yoshimura: Toyota Technological Institute, TTI, 2-12-1 Hisakata, Tempaku, 468-8511, Nagoya, Japan

being the most suitable to provide a certain type or form of graphene for specific applications [7]. However, the direct deposition of graphene onto any substrate, including its shape selection, patterning flexibility, accuracy, etc., is especially challenging. Consequently, among the post-growth processing techniques applied to graphene, transfer is often required. For CVD graphene transfer includes the application of strong chemical etchants and macroscopic mechanical manipulation. Transfer techniques are not only time and material consuming, but often detrimental to the pristine graphene properties.

Nonetheless, great advances on graphene growth and related processing have been steadily and intensively powered thanks to the interest from the industry on graphene, towards its commercial exploitation [8]. For the part that concerns graphene-based microelectronics devices, a focus on the graphene (synthesis) investigations is to fulfill certain standardization requirements, and then, in terms of processing and device fabrication. This is due to the necessity to enable integration of graphene into conventional planar technology. While the need of transferring grown graphene onto a practical substrate is undesirable, graphene patterning is an additional main concern.

Previously, we have introduced our studies on the application of focused ion beam induced deposition of Carbon (FIBID-C) for obtaining graphene materials [9,10,11,12]. First demonstration of the thermal transformation of FIBID-C into patterned graphitic layers is reported in Ref. 9. Ni material in the form of polycrystalline foil was used for the catalysis of the FIBID-C graphitization. This catalyst (Ni) and its form (foil) determine and limit the quality and extent of crystallization. Although the obtained materials had reduced crystallinity, as understood from their Raman scattering characterization, the methodology is attractive as it allows strategic placement of a finite amount of carbon precursor onto desired substrates, such as technologically relevant silicon dioxide. Additionally, due to the spatial resolution of the ion probe technique, FIBID-C can be patterned with remarkable precision [13].

Better insight on the comprehension of the mechanism of crystallization of the thin FIBID-C layers has been addressed in Ref. 10. Electron microscopy techniques, such as high resolution transmission electron microscopy (HR-TEM) and electron energy loss spectroscopy (EELS), were employed to track the two stages of FIBID-C graphitization: thermal treatment induced carbonization and metal (Ni) assisted crystallization. Cross sectional morphological imaging confirmed the finite size of the multilayer graphene crystals but also their parallel orientation with respect to the original SiO_2 support. Similarly, global probing of the

as-deposited, thermal treated and metal-assisted thermal treated FIBID-C occurred by a combination of two surface techniques, Raman scattering and X ray photoemission spectroscopy (XPS); this allowed to correlate and quantify the incomplete crystal relaxation of the graphitized layers (from Raman scattering) with the chemical bonding and contents (from XPS) [12]. The main technological aspects and flexibility of the FIBID-C platform for graphene materials growth has been summarized in Ref. 11 and includes results on the diversification of the metal catalyst in terms of both its chemical element (e.g. Cu) and its form, such as nanoparticles or thin layers.

In this present work, we continue exploiting the metal-assisted thermal treatment of FIBID-C as an approach for graphene deposition. We explore the role of iron as the metal catalyst. In terms of the catalyst form, evaporated thin iron layers in direct contact to the FIBID-C membrane are employed. The absolute and relative amounts of catalyst and C precursor necessary for graphene formation are analyzed. We demonstrate the evidence of formation of high quality single and few layer graphene, in contrast to the limited crystallinity and excess of layers obtained in previous experiments based on Ni foil catalyst [9-12].

2 Experimental Materials

Fe layers have been deposited onto 300 nm thick thermal SiO_2 on Si by using evaporation technique. Three different Fe thicknesses are tested ~10 nm, ~25 nm and ~100 nm (Figure 3). For technical reasons (i.e. the lithography mask), the Fe features are patterned having a cross-shape, which is ~10 μm in size. A conventional processing sequence is used for the fabrication of the Fe patterns which includes: resist deposition, photolithography, resist development, metal deposition and resist lift-off.

The rest of the experimental aspects of the reactor platform are similar to previously reported works [9-12]. However, it is important to remark here that the FIBID-C is deposited i) overlapped and ii) on top of designated Fe patterns fabricated on the SiO_2 surface. The shapes of the FIBID-C are 20×20 μm^2 squares; i.e. larger than the Fe features. Thicknesses of 10 nm, 20 nm, 30 nm and 40 nm are used, resulting from the chosen deposition-time, calibrated in Ref. 11, and beam conditions, as discussed next. A multibeam system JIB-4500 from JEOL has been employed. Gallium ion beam conditions are 30 kV beam voltage and a beam current of 300 pA (spot size ~42 nm). The gaseous C precursor molecules are phenanthrane. As deposited FIBID-C forms a compact partially hydrogenated DLC layer [10,12,14].

All samples have been thermally processed in vacuum (with $P < 0.4$ Pa) for 30 minutes at $T = 975$ °C using a lamp furnace (MILA 5000 from Ulvac Corp.). As in previous experiments, the heating ramp from room temperature to the target temperature takes an additional 5 minutes, and natural cooling completes the thermal treatment (~30 minutes extra). The FIBID-C processed sample is also capped during the heat treatment in the present experiments, with a blank 500 nm thick thermal SiO_2 / Si chip [9-12].

Structural and morphological characterization of the transformation of the FIBID-C layers is done by Raman scattering and scanning electron microscopy (SEM). Raman spectra are acquired by an inVia Reflex system from Renishaw, using the 532 nm laser excitation wavelength. Spot size is ~2 μm. SEM apparatus is a Hitachi S-4700 operated at 20 keV. Atomic force microscopy (AFM) has occasionally been applied for a better determination of selected topographies, *e.g.* Fe pattern thicknesses. For the AFM imaging, a scanning probe microscopy system, NanoNavi II E-Sweep from Seiko Instruments has been employed. Commercial Si probes (model TAP300AL, ~300±100 kHz, 40 N/m) from Budget Sensors Inc. are utilized in noncontact dynamic mode of operation.

3 Results and Discussion

Evidence of graphene crystal formation by means of the thermal treatment of FIBID-C using thin layer Fe patterns is shown in Figure 1. Figure 1 a) includes a Raman scattering spectrum of the center location of a ~100 nm thick Fe pattern, as indicated with an arrow in Figure 1 b). In this location, part of the as-deposited FIBID-C (~30 nm thick) transformed into graphene due to the metal-assisted thermal treatment (Figure 1 a) red line). Graphene identification can be determined from the sharpness of the peaks located at ~1585 cm^{-1} and ~2695 cm^{-1}; these peaks

correspond to the G and 2D bands which are signatures of a graphene crystal [15]. The FWHM of the 2D band is ~77 cm^{-1} which suggests that bilayer graphene has been grown. Remarkably, the absence of the D band signal (~1350 cm^{-1}) is an indication that the observed graphene flakes have a high degree of crystallinity (single crystals) and are free from contamination (*i.e.* defect-free) [16]. A zoomed in SEM image of one of the two graphene flakes is presented in Figure 1 c). The graphene flakes form round shapes and edges, in contrast with the sharp hexagonal crystals that can be attained by chemical vapor deposition (CVD) [17,18], and appear superficially flat.

It is also interesting to evaluate the crystal structure, after the thermal treatment, within FIBID-C pattern in locations which were not originally overlapped or in direct contact with the cross-shaped Fe deposits. A representative Raman scattering spectrum is plotted by the blue line in Figure 1 a). Partial in depth graphitization of FIBID-C, finite crystal size and incomplete crystal relaxation of the graphitized materials is found. These structural aspects can be understood from the bumped background of the Raman scattering signal, the significant widths of the peaks as well as the relative intensities (I) of the D and G modes [9,19], here $I_D > I_G$. It should be noted that, this crystallinity is remarkably higher than what can be obtained using only the thermal treatment of FIBID-C without any metal catalysis [9-12]. Indeed, this spectrum is very similar to the typical spectra obtained in our previous experiments using Ni foils [9-12].

Further, it is important to note that both the patterned Fe layer and the graphenized FIBID-C are highly deconstructed from their original shape, a result of the thermal treatment. Although melting is predictable for nanometer thick Fe layers at high temperature (as here 975 °C), we have observed that the pattern distortion is not strictly generated for the FIBID-C patterns when simply heat treated. However, the combination of Fe-C in direct
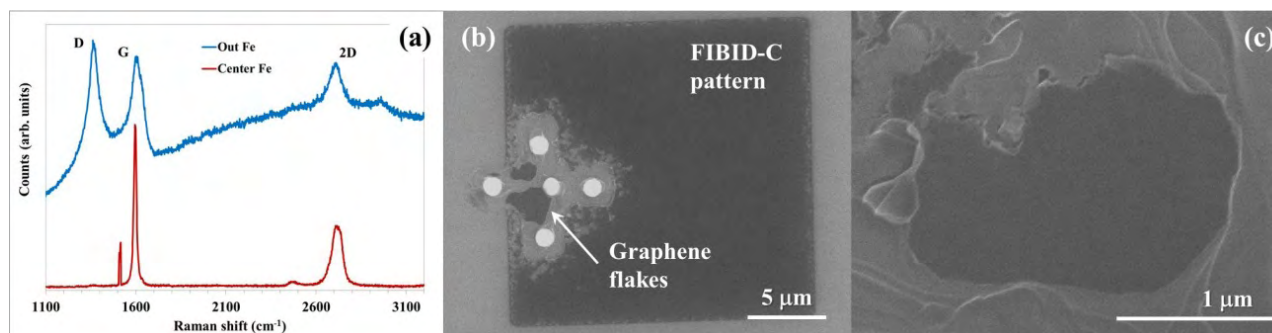
Figure 1: (a) Raman spectra of crystalline carbon obtained from the 30 nm as-deposited FIBID-C on ~100 nm thick Fe pattern after 30 minutes of thermal treatment at $T = 975$ °C. (b) General SEM image of the FIBID-C pattern and obtained graphitic materials presented in (a). (c) Detailed SEM image of one of the two single crystal graphene flakes revealed in (a) and (b).

mechanical contact at high temperature clearly promotes the decomposition of FIBID-C. Alloying is apparent, as expected from the Fe-C phase diagram [20]. More details on those changes are presented in the following paragraph.

Exemplary results of combining different layer thicknesses of Fe and FIBID-C layers are shown in Figure 2. For very thin layers, *e.g.* both the Fe and FIBID-C layers of ~10 nm thickness, the formation of small spherical Fe nanoparticles and carved FIBID-C surfaces are obtained (Figure 2 a)). The degree of graphitization of FIBID-C is again equivalent to the results for FIBID-C graphitization assisted by Ni-foils, as understood from the Raman scattering signal. The absence of a background indicates that the crystallization is uniform in depth (*i.e.* it affects the whole FIBID-C layer thickness), as shown by the blue line in the inset of Figure 2 a) and labeled as in [10]. Additionally, certain graphitization of FIBID-C is found apart from the overlapped areas of the Fe and FIBID-C patterns (labeled as "out" in the Raman spectra plot of the inset of Figure 2 a), red line). While the degree of graphitization is also limited, here FIBID-C basically maintains its pattern integrity. In the outer areas of the SEM image, small particles underneath the FIBID-C can be observed; these particles may be a result of the migration of some amount of the Fe pattern. Fe nanoparticles contribute to FIBID-C graphitization.

In Figure 2 b) the Raman spectrum of the crystalline carbon, resulting from the thermal treatment of ~20 nm as-deposited FIBID-C on ~25 nm thick Fe pattern, is shown. Here, incomplete crystal relaxation of graphene/graphite is obtained, however the inversion of the relative intensities of the D and G modes ($I_D < I_G$) indicates that the finite crystallite size increases with respect to, for example, the ~10 nm FIBID-C combined with ~10 nm thick Fe, where $I_D > I_G$ (Figure 2 a)).

In contrast, results from the thermal annealing of the as-deposited ~10 nm FIBID-C on the ~25 nm thick Fe pattern are shown in Figure 2 c). Here, no crystalline-C could be detected by Raman scattering in the area of FIBID-C overlapped with the Fe pattern. This observation suggests that FIBID-C and Fe layer have fused, likely forming iron carbides. Further, these results highlight the critical importance of both the absolute and relative amounts of iron and carbon for the graphenization process, which will be tabulated in the following paragraphs. The SEM image in Figure 2 c) also demonstrates how some Fe, for example in the form of nanoparticles, can effectively migrate (through displacement) through the FIBID-C matrix. Fe migration is observed i) as in Figure 2 c), *i.e.* carving the FIBID-C pattern, ii) rearranging underneath the FIBID-C layer (Figure 1, b)), and iii) diffusing mainly on top of the FIBID-C layer (data not shown). Similar rearrangements of the metal in combination with FIBID-C upon thermal treatment have been reported for Pt thin layers in Ref. 11.

It is interesting to analyze more in detail the relation of the amounts of carbon precursor and catalyst and their correlation with the graphitization of FIBID-C. Here, materials quantities are expressed in terms of their layer thicknesses (t), where t_C and t_{Fe}, correspond to the FIBID-C and Fe layer thicknesses, respectively. Our set of results points towards four principal features: 1) when the amount of Fe is similar or higher than the amount of FIBID-C ($0 < t_{Fe} \geq t_C$) graphitization of FIBID-C occurs, 2) the degree of crystallization depends on the absolute amounts of deposited layers; larger graphitized crystals (G_c) are obtained when using thicker layers (Gc (t_{Fe}=10 nm) < Gc (t_{Fe}=25 nm), 3) a certain minimum amount of Fe is required for the formation of graphene layers (25 nm < t_{Fe} ≤100 nm) and 4) a certain amount of FIBID-C is required for the
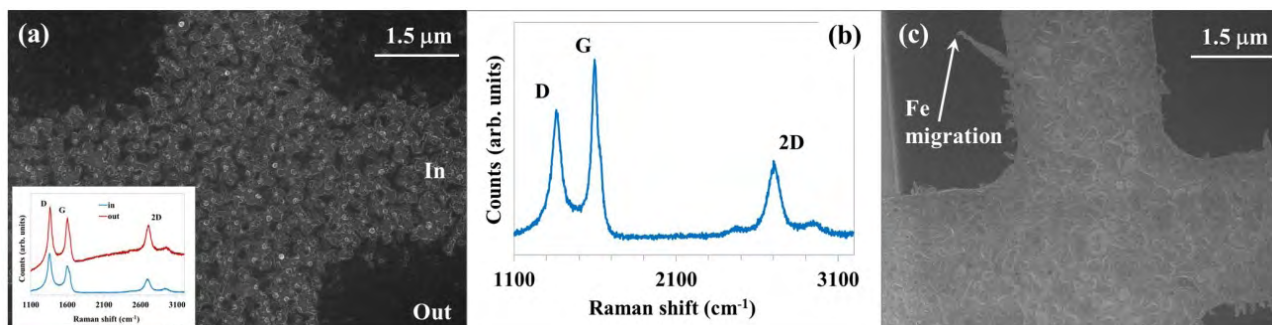
Figure 2: (a) SEM image of the products of thermal annealing as-deposited ~10 nm thick FIBID-C on a ~10 nm thick Fe pattern. Two areas are apparent and should be distinguished according to the starting materials for reference; FIBID-C deposited overlapping the cross-shaped Fe pattern (In) and directly onto the SiO_2, i.e. outside the Fe feature (Out). Inset includes respective Raman spectra in both kinds of locations. (b) Raman spectrum of crystalline carbon obtained from 20 nm as-deposited FIBID-C on ~25 nm thick Fe pattern. (c) SEM image of the materials resulting from thermal annealing of 10 nm as-deposited FIBID-C on ~25 nm thick Fe pattern. No crystalline C could be detected by Raman scattering due to an insufficient amount of carbon precursor, which promotes Fe particle mobility towards the non-overlapped FIBID-C.

detection of crystalline carbon after thermal treatment ($\sim t_C \geq 0.5 t_{Fe}$).

Figure 3 summarizes the primary trends discussed in the previous paragraph, based on materials shown in Figure 1 and 2, as well as a number of additional data. Line profile data based on AFM images of some of the as-deposited Fe patterns is included in Figure 3. AFM profiles also illustrate the finite roughness characteristics of the layers used as the catalyst of FIBID-C crystallization.

As compiled in Figure 3, single crystal graphene layers in the form of flakes are obtained when using the ~100 nm thick Fe patterns provided that a minimum amount of FIBID-C is present ($t_C > 0.2 t_{Fe}$). Additionally, when $t_C < 0.5 t_{Fe}$ crystalline carbon is not detected. In the rest of the cases, graphitic carbon forms having variable degree of graphitization are obtained. Graphitic carbon includes a range of material forms as i) only partially in-depth-graphitized FIBID-C layers (existence of background in the Raman spectra) [10], ii) variable tens of nanometer-order size crystallites (nanographene) [9], by which the size is determined by t_C/t_{Fe} and quantifiable from I_D/I_G of the Raman spectra, and iii) graphitized FIBID-C patterns, which do not keep the original integrity of the layer shape.

Based on the results presented here, a simple model for the elucidation of the mechanism of graphenization of the FIBID-C membranes *via* patterned Fe thin layer, by

means of high temperature treatment, is provided. The results indicate that the crystallization of an as-deposited amorphous FIBID-C [10,12] in the present experiments is unambiguously induced by the presence of Fe. To enable the formation of graphene flakes, complete wetting into the Fe pattern of a sufficient amount of FIBID-C is essential. We propose that the formation of the graphene crystal would proceed due to the supersaturation of Fe with C (forming iron carbide) and precipitation of atomic carbon, which in the present experimental conditions of pressure and temperature sinks in the graphite allotrop [21]. While some concerns of the thermodynamics and chemistry of the mechanism have to be studied in more detail, the possibility to use Fe as a catalyst for graphene formation is evidenced, in spite of a priori considerations [22]. The mechanism can be understood in the context of growing carbon nanotubes from catalytic Fe nanoparticles, where the formation of iron carbides has been previously demonstrated [23].

Another example which illustrates this principle is shown in Figure 4. The undesired consequence of this mechanism is the total decomposition of both the patterned Fe and the FIBID-C layers. The formation of iron silicides, in addition to the iron carbides (*e.g.* as seen in Figure 2 c)), cannot be discarded. In other words, the integrity of SiO_2 at 975 °C in the presence of Fe and C may

Catalyst & Precursor	Fe nominal thickness (nm)		
Carbon crystalline products	~10	~25	~100
~10	Graphitic carbon	X	X
~20	Graphitic carbon	Graphitic carbon	Graphene layers
~30	Graphitic carbon	Graphitic carbon	Graphene layers
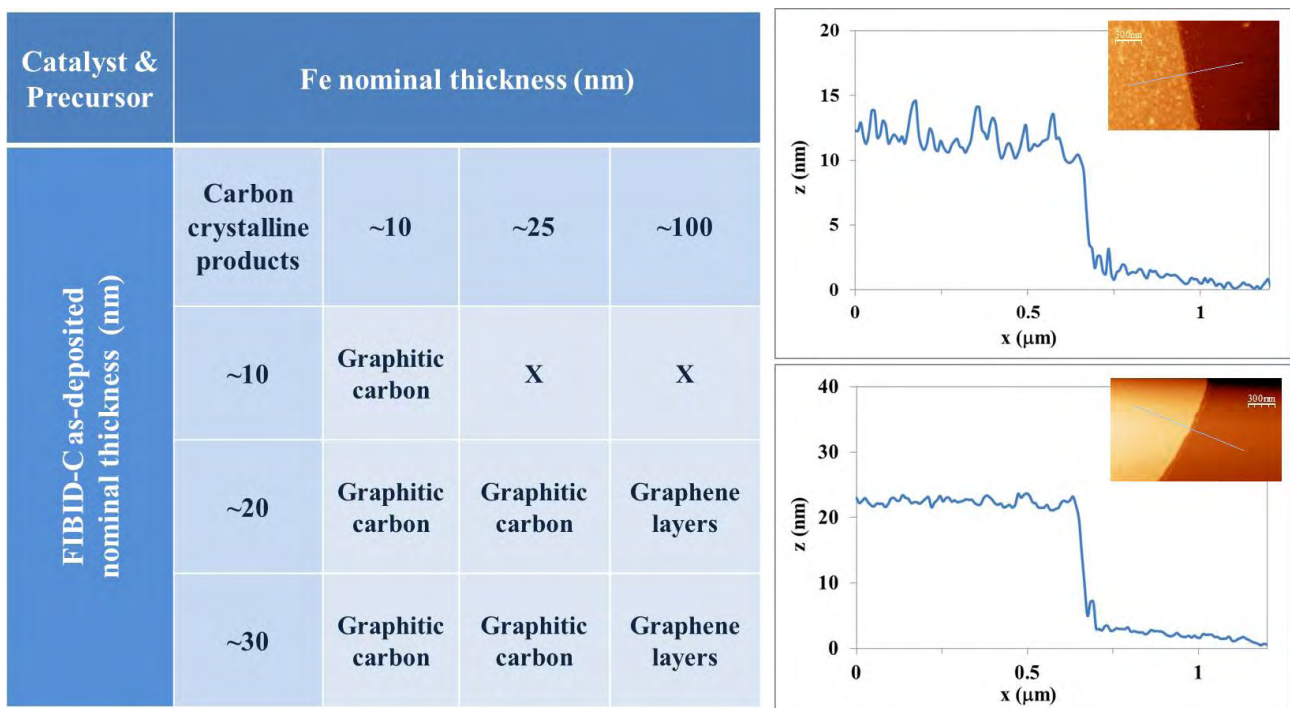
Figure 3.: Classifying table for the results of FIBID-C crystallization by thin layer patterned Fe assisted thermal treatment, as a function of as-deposited thicknesses of FIBID-C and Fe. Reference materials for thickness and roughness of the Fe layers based on AFM images are displayed on the right side. The insets included in the profiles depict the topography signal AFM images and location from where profile data are extracted.

be compromised, *i.e.* decomposition process induced by crossed chemical reactions may occur, where eventually the presence of some residual Ga from the focused ion beam would also contribute to boost the reactivity. In terms of the support for the actual deposition of graphene, the formation of terraces (Figure 4 a)) seems to be an important factor to facilitate atomic carbon nucleation and clustering, therefore forming a graphene flake (Figure 4 b)). In this case, the Raman spectrum (Figure 4 c)) indicates that deposited graphene is mostly composed of single layer graphene crystals, however the contrast in the SEM image suggests that a bilayer is covering partially some of the upper terraces (Figure 4 b), left hand side).

As demonstrated in this report, the partial decomposition of the original Fe and FIBID-C patterned layers is observed for some of the partially graphitized FIBID-C materials (graphitic carbons). This occurs primarily when Fe and FIBID-C are in direct contact; this validates the mechanism based on the phase diagrams proposed above [24]. Additionally, it highlights the sensitivity of the absolute volumes and relative percentages of catalyst and precursor masses, for obtaining graphene from a finite carbon source. The strictness of this requirement is logical as the graphene is precisely a 2D one atom thick crystal, well below the accuracy of the precursor and catalyst layer deposition. Undoubtedly, more accurate experiments would be needed to further validate and quantify this aspect.

As mentioned above, some of the graphitized products, those having limited degree of graphitization and reduced crystalline size, have structural characteristics very similar to the products of FIBID-C graphitization by Ni foil induced thermal treatment [9-12], as understood from their respective Raman spectra. Two

aspects of their similarity are worth mentioning. First, with a Fe catalyst we have been able to understand that partial crystallization can be attributed to incomplete wetting of the FIBID-C and Fe. This occurs when the Fe layer is broken into (small) particles due to heating. Since the deconstructed Fe layer is in mechanical contact with FIBID-C it also promotes localized decomposition of the FIBID-C layer, leading to confined graphitization. This mechanism may be an indication that our previous studies on Ni foil limited catalysis also occurs because of local superficial Ni-FIBID-C interaction. Second, the present results give further evidences of the possibility of 'remote' crystallization (graphitization) of the FIBID-C. In other words, we propose a certain avalanche effect starting from the actual contact of the metal catalyst with the FIBID-C, which acts as the onset of graphitization as it frees some sp^3 bonded carbons of the as-deposited FIBID-C at the metal catalyst interface. In this case, we propose that the use of point catalyst as a function of the thermal treatment time could be used to measure the spatial propagation of graphitization in FIBID-C [11].

In conclusion, there are a number of possibilities for future work based on the FIBID-C platform and its combination with thermal annealing crystallization mediated by metal catalysis. Among the aspects of the graphene reactor which clarification is pending, effect of the SiO_2 substrate and eventual contribution of residual atomic Ga are among the relevant aspects. Use of focused electron beam induced deposition (FEBID) of carbon could be an interesting option to be tested, as FEBID would provide higher purity of the carbon precursor [25,26]. Additionally, higher precision in the deposited catalyst and carbon precursor layers and their shapes would be beneficial for a higher accuracy in the
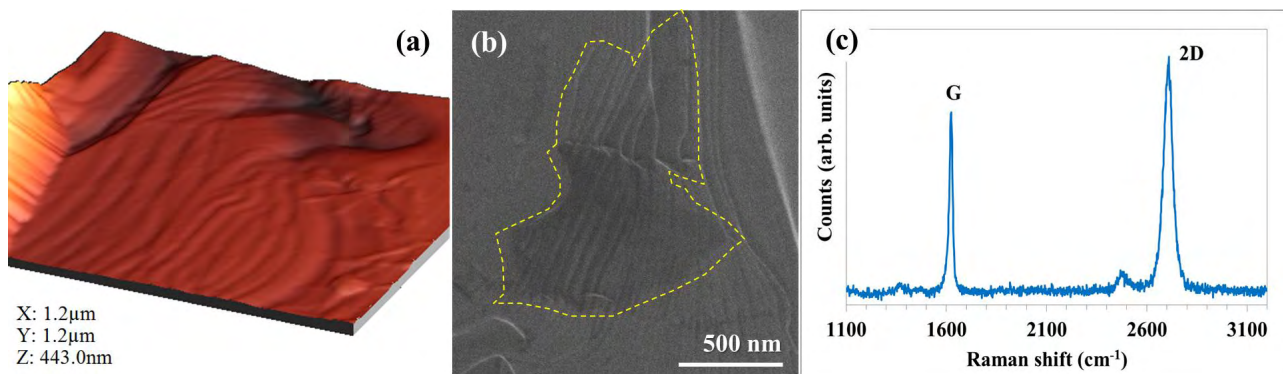
Figure 4: (a) AFM image of an area where graphene was deposited; starting from as-deposited ~40 nm thick FIBID-C on ~100 nm thick Fe. Reconstruction of Fe in the presence of carbon often results in terrace formation, where atomic carbon can cluster and sink in the form of graphene flakes. (b) Same area observed by SEM, where graphene crystal can be clearly identified due to electronic signal contrast. The yellow line is a guide for the eye to make clearer the area under discussion. (c) Raman spectra of the high quality single crystal single layer graphene is presented in (a) and (b).

quantitative determination of the amounts required for graphene formation. Consequently, optimization of the graphene flakes formation, such as increase of the grown flakes, would be made possible.

4 Conclusion

In the present work, we have validated the approach based on FIBID-C as a route for graphene deposition. In this case, patterned Fe thin layers have been used for the catalysis of graphenization and graphitization. We demonstrate the formation of high quality single and few layer graphene from FIBID-C. Additionally, we demonstrate the possibility of using Fe as catalyst for graphene deposition. The mechanism is understood as the minute precipitation of atomic carbon after supersaturation of some iron carbides formed under the high temperature treatment. However, as the graphenization mechanism is based on the complete wetting of FIBID-C and patterned Fe layers, as-deposited patterns do not preserve their original shape after the thermal treatment. In the case of obtaining partial graphitization and incomplete crystal relaxation of FIBID-C by using an Fe catalyst, strong structural similarities with our previous works based on Ni foil-assisted crystallization of FIBID-C are found. The present FIBID-C-based platform and methodology represents a suitable and practical reactor to test the potential of solid carbon sources for graphene deposition with remarkable precision and processing flexibility.

References

[1] Proposal for all-graphene monolithic logic circuits. J. Kang, D. Sarkar, Y. Khatami, K. Banerjee Appl. Phys. Lett. 103, 083113 (2013)

[2] Synthesis of graphene and its applications. W. Choia, I. Lahiria, R. Seelaboyinaa,Y. S. Kang Critical Reviews in Solid State and Materials Sciences 35, 1, 52-71 (2010)

[3] Electrostatic interactions between graphene layers and their environment. J. Sabio, C. Seoánez, S. Fratini, F. Guinea, A. H. Castro Neto, F. Sol Phys. Rev. B 77, 195409 (2008)

[4] Grains and grain boundaries in single-layer graphene atomic patchwork quilts. P. Y. Huang, C. S. Ruiz-Vargas, A. M. van der Zande, W. S. Whitney, M. P. Levendorf, J. W. Kevek, S. Garg, J. S. Alden, C. J. Hustedt, Y. Zhu, J. Park, P. L. McEuen, D.A. Muller Nature 469, 389–392 (2011)

[5] Electric Field Effect in Atomically Thin Carbon Films. K. S. Novoselov, A. K. Geim, S. V. Morozov, D. Jiang, Y. Zhang, S.V. Dubonos, I. V. Grigorieva, A. A. Firsov, Science 306, 666–669 (2004)

[6] Production: Beyond sticky tape. R. Van Noorden Nature 483, S32–S33 (2012)

[7] Graphene: synthesis and applications, P. Avouris, C. Dimitra-kopoulos Materials Today 15, 3, 86–97 (2012)

[8] A roadmap for graphene. K. S. Novoselov, V. I. Fal'ko, L. Colombo, P. R. Gellert, M. G. Schwab, K. Kim Nature 490, 192–200 (2012)

[9] Synthesis of Patterned Nanographene on Insulators from Focused Ion Beam Induced Deposition of Carbon. G. Rius, N. Mestres, M. Yoshimura, Journal of Vacuum Science and Technology B 2012, 30(3) 03D113-1

[10] Focused ion beam as a tool for graphene technology: Structural study of processing sequence by electron microscopy. G. Rius, A. H. Tavabi, N. Mestres, O. Eryu, T. Tanji, M.Yoshimura Jpn. J. Appl. Phys. 53 02BC22 (2014)

[11] Metal-Induced Crystallization of Focused Ion Beam-Induced Deposition for Functional Patterned Ultrathin Nanocarbon. G. Rius, X. Borrisé, N. Mestres FIB Nanostructures Lecture Notes in Nanoscale Science and Technology Volume 20,123-159 (2013)

[12] Nanographene patterns from focused ion beam induced deposition. Structural characterization of graphene materials by XPS and Raman scattering. M. Castellino, G. Rius, A. Virga, A.Tagliaferro. Handbook of Graphene Science, Taylor and Francis Ed. – (Book chapter. Under Review)

[13] Three-dimensional nanostructure fabrication by focused-ion-beam chemical vapor deposition. S. Matsui, T. Kaito, J. I. Fujita, M. Komuro, K. Kanda,Y. Haruyama J. Vac. Sci. Technol. B 18, 3181 (2000)

[14] Carbon nanopillar laterally grown with electron beam-induced chemical vapor deposition. J. Fujita, M. Ishida, T. Ichihashi, Y. Ochiai, T. Kaito S. Matsui J. Vac. Sci. Technol. B 21, 2990 (2003)

[15] Raman Spectrum of Graphene and Graphene Layers. A. C. Ferrari,J. C. Meyer, V. Scardaci, C. Casiraghi, M. Lazzeri, F. Mauri, S. Piscanec, D. Jiang, K. S. Novoselov, S. Roth, A. K. Geim PRL 97, 187401 (2006)

[16] Raman spectroscopy of graphene and graphite: Disorder, electron–phonon coupling, doping and nonadiabatic effects. A. C. Ferrari Solid State Communications 143, 1–2, 47–57 (2007)

[17] Edge-controlled growth and kinetics of single-crystal graphene domains by chemical vapor deposition. T. Ma, W. Ren, X. Zhang, Z. Liu, Y. Gao, L.-C. Yin, X.-.L. Ma, F. Ding, H.-M. Cheng Proc. Natl. Acad. Sci. USA 20386-20391 (2013)

[18] Chemical Vapor Deposition of Graphene Single Crystals. Z. Yan, Z. Peng, J. M. Tour Accounts of Chemical Research Article ASAP (2014)

[19] Raman Spectroscopy of Graphene Edges. C. Casiraghi, A. Hartschuh, H. Qian, S. Piscanec, C. Georgi, A. Fasoli, K. S. Novoselov, D. M. Basko, A. C. Ferrari Nano Lett., 9, 4, 1433–1441 (2009)

[20] The P, T Phase and Reaction Diagram for Elemental Carbon. F. P. Bundy Journal of Geophysical Research, 85, B12, 6930-6936 (1980)

[21] Phase Diagram of Quasi-Two-Dimensional Carbon, From Graphene to Diamond. A. G. Kvashnin, L. A. Chernozatonskii, B. I. Yakobson, P. B. Sorokin Nano Lett. 14 (2), 676–681 (2014)

[22] The surface science of graphene: Metal interfaces, CVD synthesis, nanoribbons, chemical modifications, and defects. M. Batzill Surface Science Reports 67, 3–4, 1, 83–115 (2012)

[23] Prediction of carbon nanotube growth success by the analysis of carbon–catalyst binary phase diagrams. C. P. Deck, K. Vecchio Carbon 44, 2, 267–275 (2006)

[24] Growth of large-area graphene films from metal-carbon melts. S. Amini, J. Garay, G. Liu, A. A. Balandin, R. Abbaschian J. Appl. Phys. 108, 094321 (2010)

[25] Gas-assisted focused electron beam and ion beam processing and fabrication. I. Utke, P. Hoffmann, J. Melngailis J. Vac. Sci. Technol. B 26, 1197 (2008)

[26] Comparison of FIB-CVD and EB-CVD growth characteristics. J. Igaka, K. Kanda, Y. Haruyama, M. Ishida, Y. Ochiai, J.-I. Fujita, T. Kaito, S. Matsui Microelectronic Engineering 83, 4–9, 1225–1228 (2006)